Time Evolution of Mixing in the Staggered Herringbone Microchannel

Article *in* Modern Physics Letters B · November 2011

DOI: 10.1142/S0217984911026826

2 authors, including:

Miron Kaufman
Cleveland State University

Modern Physics Letters B

TIME EVOLUTION OF MIXING IN THE STAGGERED HERRINGBONE MICROCHANNEL

PETRU S. FODOR

Physics Department, Cleveland State University
Cleveland, Ohio 44115, USA
p.fodor@csuohio.edu

MIRON KAUFMAN*

Physics Department, Cleveland State University
Cleveland, Ohio 44115, USA
m.kaufman@csuohio.edu

Received Day Month Day
Revised Day Month Day

Patterning ridges on the surface of microchannels has been found to be a viable strategy to induce mixing in straight channels, despite their characteristically small Reynolds numbers. In order to identify the fundamental characteristics of the advection process we evaluate the time evolution of the Rényi entropy associated with the spatial distribution of tracers carried by an incompressible fluid moving through such channels. It is found that independent of the channel surface geometry and of the Reynolds number, the time evolution of the Rényi distributive entropy follows a universal behavior described by a logarithmic increase with time, with a slope close to unity. On the other hand an analysis of the Shannon mixing entropy evaluated from the time evolution of the position of two tracer species moving through the channel, reveals a crossover between two different mixing mechanisms: one dominated by the stretching of the interface between the flow regions containing different tracers, and the other dominated by chaotic mixing induced by counter-rotating transversal flows.

Keywords: Microchannels; staggered herring bone mixer; mixing entropy.

1. Introduction

Given the rapid developments in the ability to manipulate and engineer fluid flows on the microscale, microfluidic based devices are currently envisioned as a technological platform capable of providing increased throughput and deploy-ability in applications covering chemical and biological sensing[1], chemical synthesis[2], protein analysis[3] and drug discovery.[4] For any of these applications one of the central requirements for their successful operation is the mixing of two or more fluid components. However on the microscale this is challenging because at the low Reynolds numbers characteristic to microfluidic devices, the fluid flow is laminar and thus the mixing relies on the relatively slow molecular diffusion.[5] In these conditions the time and spatial scales necessary for

* Present address: Physics Department, Cleveland State University, 2121 Euclid Avenue, Cleveland, Ohio 44236, USA.

the mixing to occur in the required concentration ranges, become prohibitively large for most applications.

The most popular strategy for promoting mixing in micrometer scale devices, was pioneered by Stroock *et al*.[6], who used repeating sequences of asymmetric staggered herringbone (SHB) shaped ridges, patterned on the bottom of rectangular microchannels. In this geometry, the ridges and grooves of the SHB design disturb the laminar flow of the fluid along the longitudinal axis of the microchannel by inducing counter-rotating transversal flows that promote mixing between different fluid components. The advantages of the SHB design are multiple. Besides its ability to achieve good mixing on lengths scales of the order of a few centimeters, making it relevant for lab-on-a-chip applications, it is also simple enough to be manufactured in a two step soft lithography process followed by replica molding.[7] Also, the SHB reliance on geometrical features makes it a passive design that achieves good mixing quality without requiring external power sources, besides the pressure gradient between the inlet and the outlet of the device.

The geometrical simplicity of these designs makes them particularly suitable for computational modeling of the fluid flows[8-10] or even simple analytical models.[11] The many computational studies concerned with the SHB design have been focused on investigating the influence on the mixing quality of geometrical features including: the groove depth to channel height ratio[12], the number of grooves per half cycle[10], the width of the grooves[13], the ratio between the width of the grooves with respect to the width of the ridges[14], or the ratio of the long arm to the short arm of the grooves.[15] Those studies have focused on the steady state analysis of the fluid flow and the evaluation of the quality of mixing from the positions of tracer species carried by the fluid in cross-sections distributed along the length of the channel. The entropy is the unique rigorous measure of the homogeneity of a system, and it has been previously used to define a mixing measure for the fluid flows in microchannels[16-19] from steady state cross sections of the tracers positions.

While this two dimensional approach has the advantage that the cross - sectional images of the tracers can be correlated with experimental confocal microscopy images of fluorescent dyes carried by the fluid[6], we expect to gain further insights into the dynamics of mixing by evaluating mixing in three dimensions. In the current work we are evaluating the time evolution of the Rényi entropy for a system of massless and non-interacting tracers (passive scalars) carried by the fluid flow through rectangular microchannels. This study allows us to calculate the rate of entropy change and correlate it with the underlying mixing mechanisms.

1.1. *Fluid flow simulations*

The basic geometrical structure used in this study is a rectangular microchannel with a length of 5000 μm, a width of 200 μm and a height of 150 μm. For the SHB design an alternating set of asymmetric V – shaped grove/ridge patterns are placed on the channel bottom surface (Fig. 1). The geometrical parameters of the SHB surface patterns are as follows: groove/ridge width = 125μm/50 μm; the ratio between the height of the ridge and that of the channel is 0.25; and the short arm/long arm ratio for the ridges is 2/3. Each cycle of the SHB consists of five herringbones that have the short segment on the left and the long segment on the right, followed by five more herringbones with the short segment on the right and the long segment on the left, that serve to deflect the fluid flow. These geometrical parameters correspond to the optimized performance in terms of mixing quality for the rectangular microchannel considered.[20]

For obtaining the velocity fields for the geometries investigated, the finite element analysis package COMSOL Multiphysics and its Chemical Engineering Module were used.[20,21] The flow fields for each channel are obtained by solving the Navier – Stokes equations of motion for an incompressible Newtonian fluid:

$$\rho\left[\frac{\partial \mathbf{u}}{\partial t}+(\mathbf{u}\cdot\nabla)\mathbf{u}\right]=-\nabla p+\eta\nabla^{2}\mathbf{u}\,. \tag{1}$$

$$\nabla\cdot\mathbf{u}=0\,. \tag{2}$$

where ***u*** is the velocity vector, ρ is the fluid density, η is the fluid viscosity, t is the time, and p is the pressure. Typically, the values for the density and the viscosity are set to those for water at room temperature, i.e. 10^3 kg/m^3 and 10^{-3} kg/(m s), respectively. The equations are solved for the steady state flow for a pressure driven fluid. The boundary conditions are a 0.01 m/s inlet velocity (corresponding to the Reynolds number value equal to one) oriented along the longitudinal axis of the channel, zero pressure at the outlet, and no-slip at all the solid surfaces. The flow field equations are solved using a generalized minimal residual method (GMRES) iterative solver with a geometrical multigrid pre-conditioner and a Vanka algorithm for the pre- and post-smoothing. The typical number of tetrahedral elements in the mesh used is 150,000, which in the limit of low Reynolds numbers ensures that the element size is sufficiently small for the solution to be independent on the mesh.

1.2. *Particle tracing*

In order to compute the time evolution of the entropies associated with the fluid flow in this geometry, the trajectories of up to 15,000 massless tracer particles released across the inlet of the channels is computed by using a Lagrangian particle tracing method. The particle trajectories are obtained by solving the motion equation for each particle:

$$\frac{d\vec{r}}{dt}=\vec{u}(\vec{r})\,. \tag{3}$$

where the velocity $\vec{u}(\vec{r})$ at each location is obtained by interpolating through the velocity field solution obtained by solving the Navier – Stokes equation using the finite element analysis package COMSOL. The integration of the motion equation for each particle was done using a standard Runge - Kutta algorithm with fixed time steps, with the time allowed being the time necessary for the fastest particle to exit the channel.

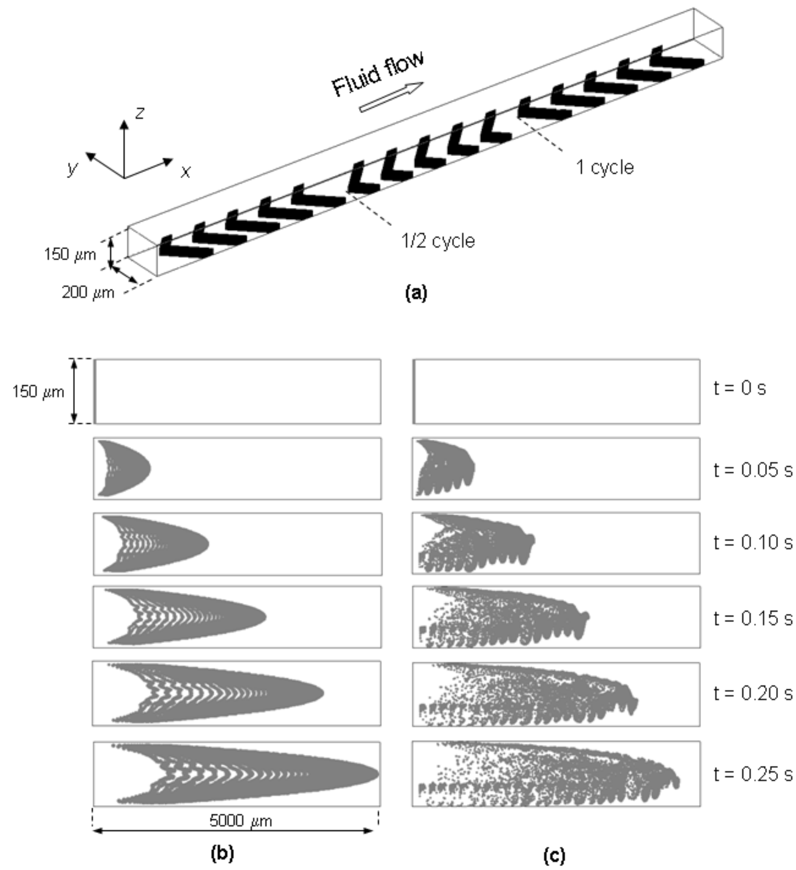

Fig. 1. (a) Staggered herringbone mixer (SHB) design (only part of the channel is shown). Time snapshots of the particles position within the microchannel (b) for a design without surface patterning and (c) for the SHB design.

Typical time evolutions for sets of particles released at the inlet are shown in Fig 1b. For a channel without any ridges on the surface the observed pattern matches the parabolic one expected for laminar flow in a simple rectangular shaped channel with known pressure gradient between the inlet and the outlet. For the SHB, the particle profiles deviate noticeably from the parabolic profiles due to the transversal flows that are generated as the fluid is pressure driven over the slanted grooves and ridges. Thus while the fluid flow is still laminar the streamlines are not simply straight lines as they reflect the non-axial components of the velocity field at different positions within the volume of the channel.

2. Results and Discussion

Knowledge of the time dependent position of the massless tracers is used to evaluate the entropy associated with their fluid driven distribution within the channels. The volume of the channel is divided into M equal sized bins, labeled $j = 1,2,\ldots,M$, and the number of particles n_j in each bin is computed.[22] The probability p_j of finding a particle in the bin labeled j is. $p_j = n_j/N$ where N is the total number of particles. The Rényi entropy depends on a parameter β[23] according to:

$$S(\beta) = \frac{1}{1-\beta}\ln\left(\sum_{j=1}^{M} p_j{}^{\beta}\right). \tag{4}$$

In the limit $\beta \to 1$ the equation (4) reduces to the Shannon information entropy[24]:

$$S(1) = -\sum_{j=1}^{M} p_j \ln p_j \ . \tag{5}$$

The above entropy relations quantify the spatial distribution of particles within the channels without regard to their type. If a number C of different species are involved, the entropy is the sum of the distributive entropy associated solely with the spatial distribution of the particles without regard of species, and a mixing entropy, associated only with the relative concentration of the different types of particles at any location:

$$S_{total} = S_{distributive} + S_{mixing} \ . \tag{6}$$

where:

$$S_{distributive} = -\sum_{j=1}^{M} p_j \ln p_j \ . \tag{7}$$

and:

$$S_{mixing} = -\sum_{j=1}^{M} p_j \left(\sum_{c=1}^{C} p_{c/j} \ln p_{c/j}\right). \tag{8}$$

where p_j is the fraction of all particles that are in bin j. The conditional probability $p_{c/j}$ is the fraction of particles of type c in bin j out of all particles in bin j. The lowest value ($S_{mixing} = 0$) corresponds to each bin containing at most one type of particle, i.e. perfect segregation between the particles. Its largest value ($S = lnC$) corresponds to the situation in which bins containing particles have an equal number of particles from each species, i.e. $p_{c/j}$ are all equal to each other in these bins. Physically this corresponds to the uniform distribution of species through the system and their perfect mixing. By normalizing the mixing entropy S_{mixing} by lnC, one can define a mixing index varying from 0 (perfect segregation) to 1 (perfect mixing).

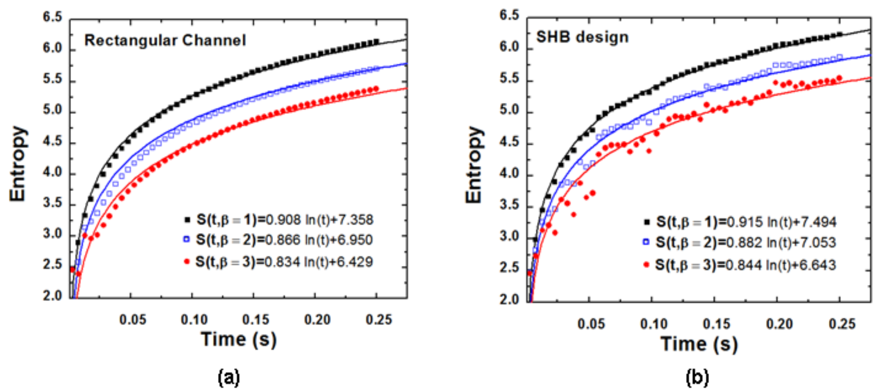

Fig. 2. (a) Renyi entropy versus time (a) for a design without surface patterning and (b) for the SHB channel.

2.1. *Distributive Rényi entropy*

For the entropic calculations the total volume of the channels is divided in 1200 cubic bins with 50 μm sides and then entropy is evaluated by evaluating the particle distribution in each bin.

For all the channels investigated the time evolution of the distributive entropy, which is determined only by the probabilities p_j of finding particles in the bin j is well described by a logarithmic dependence (Fig. 2) of the form:

$$S_{distributive} = a\ln(t) + b\,. \tag{9}$$

A seen in Fig. 3, the dependence on β of both the a and b entropy coefficients is almost identical for the channels without surface patterning, referred as rectangular channels, and the channels with SHB structures on their bottom surface. For both channels the a and b coefficients depend relatively weakly on β, with the rate of entropy change $a = dS/d(\ln t)$ decreasing from 0.94 to about 0.84 as β takes values between 0 and 3. While at first this might be surprising given the differences between the noticeable trajectories of the tracers in the two types of channels, one has to notice that in both cases the fluid flow is still laminar with the main contribution to the total entropy increase being determined by the pressure driven advection along the axis of the channel.

2.2. *Analytical model*

In order to get some insight into the logarithmic time dependence of the distributive entropy, we look at the laminar convection of particle tracers by a fluid confined between two infinite parallel plates separated by a distance W. For zero Reynolds number the Navier Stokes equation yields the parabolic profile:

$$x = \frac{4v_{\max}t}{W^2}\,y(W-y)\,. \tag{10}$$

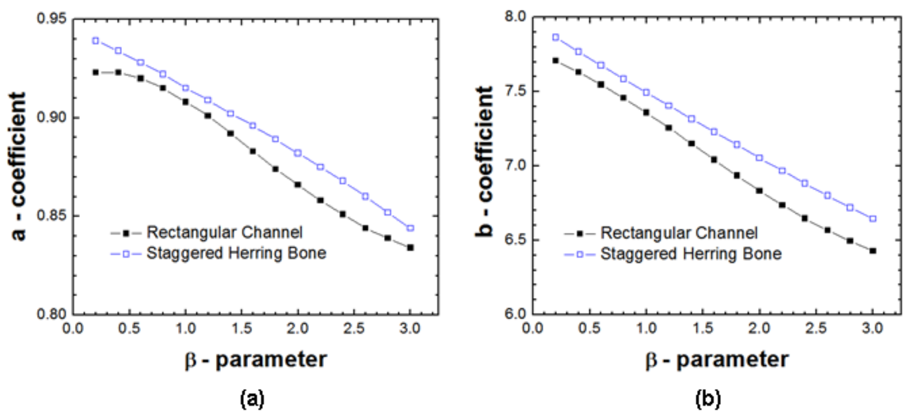

Fig. 3. β parameter dependence of the (a) *a* and (b) *b* coefficients describing the logarithmic time dependence of the entropy.

where v_{max} is the maximum speed, i.e. the speed of the fluid midway between the plates. At t = 0 all N tracer particles are at x = 0 and the density of tracers is ρ_0 = N/W. At time t the straight line becomes the parabola and the density of tracers is:

$$\rho = \frac{\rho_0}{\sqrt{(\frac{dx}{dy})^2 + 1}} \,. \tag{11}$$

where $\frac{dx}{dy} = \frac{4v_{\max}t}{W^2}(W - 2y)$.

The probability p to find a tracer is nonzero only on the parabolic front where it is:

$$p \approx \frac{\rho ds}{N} \,. \tag{12}$$

where ds is the infinitesimal length.

To calculate the distributive Rényi entropy we start by estimating the sum on the right hand side of Eq (4):

$$\sum p^\beta \approx \oint_{parabola} ds \frac{\rho^\beta}{N^\beta} \Delta y^{\beta-1} = \left(\frac{\Delta y \rho_0}{N}\right)^{\beta-1} G(\beta,\tau) \,. \tag{13}$$

where the sum on the left hand side is evaluated only for bins situated along the parabolic profile. The dimensionless time is $\tau = 4v_{max}t/W$ and:

$$G(\beta,\tau) = \frac{1}{2\tau}\int_{-\tau}^{\tau} (u^2 + 1)^{(\beta-1)/2} \,. \tag{14}$$

The Renyi entropy obtained from Eqs. (4) and (13) is:

$$S(\beta) = \ln(W / \Delta y) + \frac{1}{1-\beta}\ln(G(\beta,\tau)) . \tag{15}$$

For β = 1 we get the Shannon entropy:

$$S(1) = \ln(W / \Delta y) + g(\tau) . \tag{16}$$

where:

$$g(\tau) = \frac{1}{2}\ln(\tau^2 + 1) - 1 + \frac{a\tan(\tau)}{\tau} . \tag{17}$$

We next determine the asymptotic long time behavior of the entropy. For $\tau >> 1$ the integral in the definition of the function G is finite for $\beta > 2$ and diverges for $\beta < 2$:

$$\begin{aligned} &\int_{-\tau}^{\tau} (u^2+1)^{(\beta-1)/2} \propto \mathit{finite} \quad \mathit{if}\, \beta > 2 \\ &\int_{-\tau}^{\tau} (u^2+1)^{(\beta-1)/2} \propto \tau^{2-\beta} \quad \mathit{if}\, \beta < 2 \end{aligned} . \tag{18}$$

Using Eq. (18) and (14) we find the asymptotic behavior of $G(\beta,\tau)$ for $\tau >> 1$:

$$\begin{aligned} &G(\beta,\tau) \propto \tau^{1-\beta} \quad \mathit{if}\, \beta \le 2 \\ &G(\beta,\tau) \propto \tau^{-1} \quad \mathit{if}\, \beta > 2 \end{aligned} . \tag{19}$$

Finally the long time asymptotic behavior of the Rényi entropy is obtained from equations (15) and (19):

$$\begin{aligned} &S(\beta) \approx \ln\tau \quad \mathit{if}\, \beta \le 2 \\ &S(\beta) \approx \frac{1}{\beta-1}\ln\tau \quad \mathit{if}\, \beta > 2 \end{aligned} . \tag{20}$$

In conclusion the amplitude a of the logarithm, see Eq. (9) is:

$$\begin{aligned} &a = 1\, \mathit{for}\beta \le 2 \\ &a = \frac{1}{\beta-1}\mathit{for}\beta > 2 \end{aligned} \tag{21}$$

It is also noteworthy that for *β = 0* the function G gives the length L of the parabola:

$$\frac{L}{W} = G(0,\tau) = e^{\Delta S(0)} = \frac{1}{2\tau}[\frac{1}{2}\ln\frac{\sqrt{\tau^2+1}+\tau}{\sqrt{\tau^2+1}-\tau} + \tau\sqrt{\tau^2+1}]. \tag{22}$$

For long times L/W ~ τ/2.

Because our channels are finite the above analysis gives only a qualitative description of the observed dependencies. Nevertheless, based on the above discussion, it is apparent that the logarithmic time evolution of the entropy is characteristic to a pressure driven convection process in straight channels. Moreover, the analysis shows that the entropy coefficient *a* for such a process depends only on the parameter *β*, while the *b* coefficient is influenced not only by the initial conditions and bin size but also by the maximum speed of the fluid for a given geometry and pressure gradient. This can be easily observed for the rectangular channels described, from the dependence of these coefficients on the Reynolds number. When the fluid speed through the channel is changed in the range 0.001 to 0.1 m/s, the entropy coefficients *a* and *b* evaluated from the best fits to the entropy data, show markedly different behaviors (Fig. 4). While as expected, see Eq (21), the *a* coefficient is essentially independent on the fluid speed (Reynolds number), the *b* coefficient increases with the Reynolds number of the channels for both rectangular channels with ridges (SHB design) or without ridges.

Logarithmic time dependences of the entropy has been observed previously[25] for polymer extrusion, a process that is equivalent to a flow driven not only by a pressure gradient but also by dragging of a moving wall. In that case the mixing rate *a* depends on the Renyi parameter β. In the case of a one dimensional diffusive process the rate of entropy increase is *a* = 0.5, independent of β. By contrast we find that for the microchannel the mixing rate *a* is almost independent of β and quite close to unity.

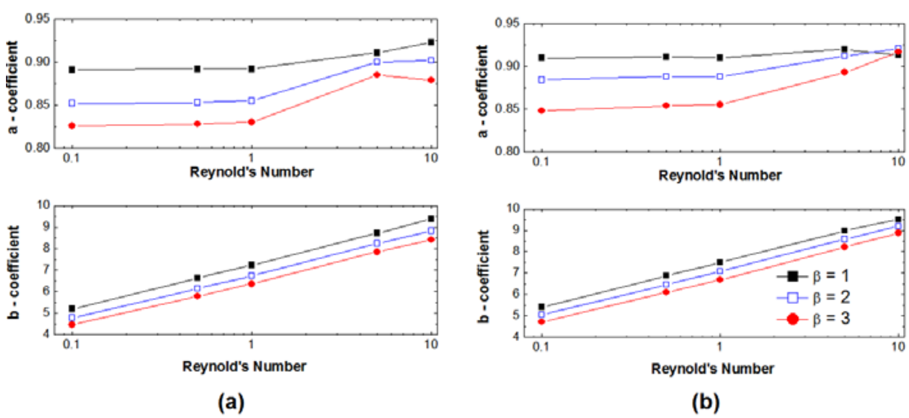

Fig. 4. Dependence of the entropy coefficients on the Reynold's number (a) channel without ridges, and (b) SHB channel.

2.3. *Shannon mixing entropy*

In order to evaluate the mixing entropy, two types of tracers are released at the inlet of the channels. The two types of tracers are initialized on separate sides of the rectangular inlet with a well defined separating interface. For the channel without any surface patterns, because the streamlines are simply straight lines parallel to the longitudinal axis of the channel, the regions occupied by the different tracers remain spatially distinct throughout the advection process and separated by the median plane of the channel. On the other hand, simple visual analysis of the particle distribution in the SHB design indicates that the presence of the ridges on the channel floor induces a crossover of particles between the two sides of the channel promoting the mixing of the two species of passive scalars (Fig. 5). Thus, even if as discussed in the preceding section the distributive entropy is not measurably affected by the presence of the ridges on the channel surface, the same behavior is not expected for the evaluation of the mixing entropy.

For simplicity only the Shannon entropy (Eq. 4) is evaluated for sets of up to 15000 particles (up to 7000 of each species). While as expected, the mixing entropy for the channel without ridges is zero, for the staggered herring bone design the mixing entropy shows a monotonic increase with time, with three distinct stages. Before any analysis one has to notice that the mixing entropy is sensitive to the scale of observation (bin size). As the number of bins is increased from 1200 to 15,000, the mixing entropy decreases (Fig. 5c). This is consistent with the decrease in the probability to find particles of different species in the same bin as the size of the bin is decreased. Nevertheless, for a sufficient number of particles the time dependence of the entropy is qualitatively the same for all the observation scales employed.

The first stage in the time evolution of the mixing entropy is characterized by a sharp incline, but a very short time span which corresponds to the particles moving over the first ridge/grooves features on the channel floor. This is a direct consequence of the transversal flows induced as the fluid moves across the anisotropic resistance profiles presented by the surface patterns. These transversal components disturb the motion of the particles along the longitudinal direction of the channel and promote particle movement across the initial interface (median plane of the channel) between the regions containing different types of tracers. The stretching and the distortion of the interface between these regions is reflected by a finite mixing of particles of different species in the bins in the immediate vicinity of the interface. However, as seen in the time evolution of the entropy the mixing index saturates very fast, because the mixing is still limited only to the finite number of bins near the interface and does not occur through the whole volume of the fluid. Experimentally this situation is equivalent with that of slanted groove micromixers which despite promoting transversal flows exhibit poor mixing quality.[26]

On the other hand for times $t > 0.1$ s, the plateau in the mixing index is followed by a sharp increase in the mixing entropy, described by a power law $S_{mixing} \sim t^{3/2}$, which at least for the length of the channels considered does not saturate. It is observed that the transition to this regime occurs sharply at the beginning of the second cycle of the SHB

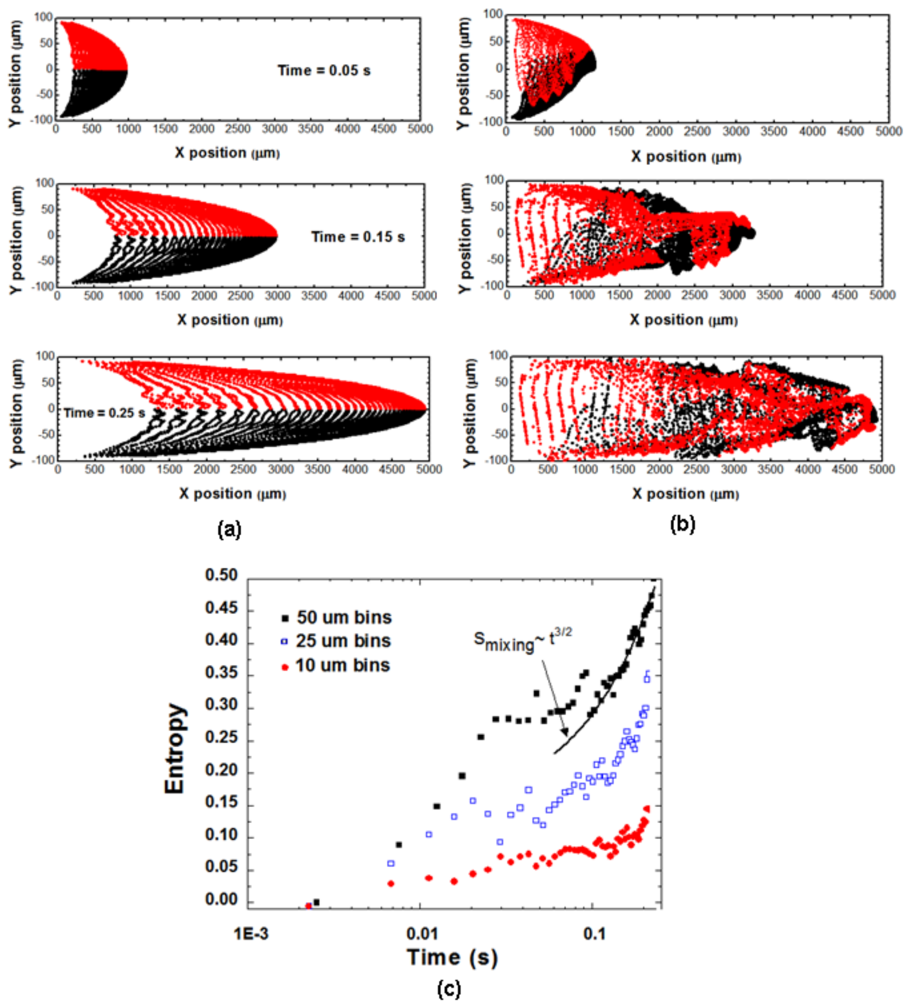

Fig. 5. Two – particle tracing in a (a) channel without ridges and (b) SHB channel; (c) Time evolution of the mixing entropy for an SHB design ($S_{mixing}/\ln(2) = 1$ corresponds to perfect mixing).

which corresponds to the exchange of the center of rotation of the counter - rotating flows induced by the asymmetric grooves.

In order to gain insight in the origin of this behavior we have explored the evolution of the interface between the two regions containing different tracers by following the evolution of a set of 1500 particles initially placed at this interface. A qualitative analysis of the interface (Fig. 6) shows that as the particles propagate along the channel the geometrical line defined by them stretches not only along the longitudinal direction of the channel, but also throughout its volume.

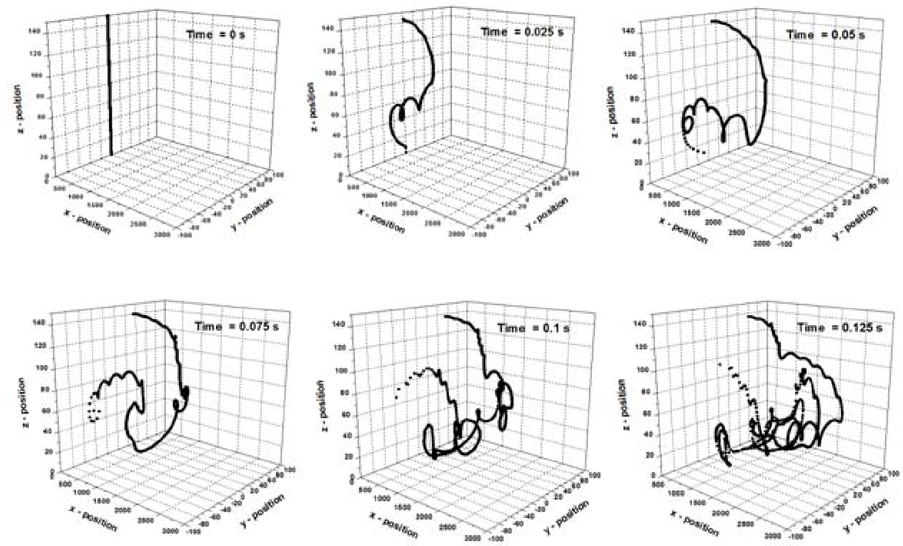

Fig. 6. Particle tracing for the interface between regions containing different tracers.

For times smaller than 0.1 s corresponding to the movement of particles only above the first cycle of ridges, the line of particles is still geometrical connected, with the particles still preserving their correlation with their initial nearest neighbors. Past the beginning of the second SHB cycle, the inter connectivity of this line is broken leading to multiple interfaces between regions with different types of tracers. In essence this corresponds to a transition between a mixing mechanism that is dominated by the exchange across a well defined interface, to a mixing occurring in the entire volume of the fluid. A measure of the correlation between each particle and its initial neighbors can be expressed by calculating the time dependence of the average Euclidean distance between the particles carried by the fluid:

$$\Delta r(t) = \frac{1}{N-1}\sum_{j=1}^{N}\left|\vec{r}_{t,j+1} - \vec{r}_{t,j}\right| . \tag{23}$$

where N is the number of particles and the $\vec{r}_{t,j}$ are the time dependent position vectors of the particles. Figure 7 shows the time dependence of this average distance for channels without surface patterns and for the SHB design. The distance is evaluated by computing the position of a set of 1500 particles released at the inlet along a vertical line corresponding to the initial interface between the regions containing different tracers. Our results for the rectangular channel overlap almost perfectly on the analytical formula for the $\Delta r(t)$ obtained assuming laminar incompressible fluid flow and calculating the length of the parabola described by the particle front as it moves through the channel.

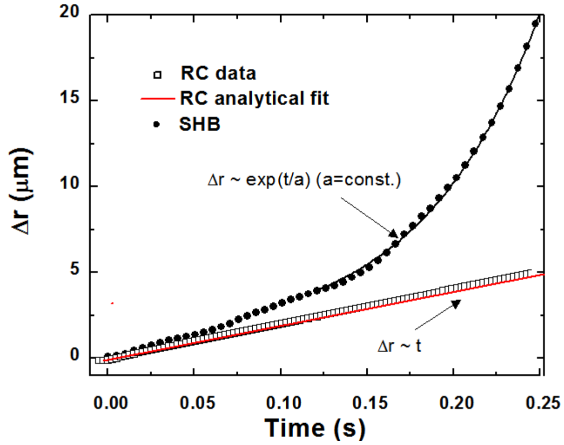

Fig. 7. Time evolution of the average distance between the nearest neighbors.

In this case, in the long time approximation, the average distance between the particles converges to quasi - linear dependence of time: $\Delta r \sim (2v_{max}t)/N$ where v_{max} is the speed along the central axis of the channel and is determined by the pressure gradient between the inlet and outlet, and N is the total number of particles.

In contrast, the nearest neighbor average distance for the SHB design has a much stronger dependence on time. While in the small time limit $t < 0.05$ s, it increases with a slope close to the one for the channel without ridges, in the long time limit $t > 0.13$ s its increase exponential: $\Delta\vec{r} \sim e^{t/a}$ with a ~ 0.07s. The crossover time coincides well with the start of the increase in the mixing entropy. This rapid increase in the average distance, signals the breaking of the correlation between the particles in the original chain in their mixing throughout the volume of the fluid. In fact the time dependence of the distance between the particles is directly related with the Lyapunov exponents associated with the divergence of the particle trajectories.[27] While a calculation of the exponents is not attempted, it is inferred from the divergence of the Euclidean distance that the Lyaponov exponents are positive, signaling chaotic flows.

3. Conclusion

We have investigated the time evolution of the entropy associated with the fluid flow in microchannels. The dominant component of the entropy, the distributive entropy associated with the spatial distribution of the tracers through the channels, is found to follow a universal behavior described by a linear increase with *ln(time),* with a slope that is independent on the presence or absence of patterned ridges on the microchannel's bottom surface. Nevertheless, the mixing entropy associated with the mixing of two species of tracers, which is essentially zero for an undisturbed laminar flow, has a more complicated time evolution for an SHB design. A clear crossover between two mixing regimes is observed. An analysis of the relative distance between the tracer particles as a function of time indicates that the crossover is associated with the transition from a regime in which the mixing is localized at the initial interface between the two tracer species, to a regime in which the mixing is takes place throughout the entire volume of the fluid. The second mixing mechanism has the characteristics of a chaotic process and is triggered by the change in the rotation center of the transversal flows induced by the asymmetric groves on the channel flow. The computational evaluation of the time evolution of the entropy provides insights into the dynamic mixing in microchannels that are very difficult to achieve experimentally, and thus can provide a supplementary tool for optimizing their mixing performance. For example, given that the dominant mixing mechanism is triggered by the change in the center of rotation of the transversal flows, it is justifiable to explore strategies in which non-periodic[17,20,22] sets of groove/ridge structures are used.

Acknowledgments

This research was supported by a grant from the Cleveland State University.

References

1. G.M. Whitesides, *Nature* **442** (2006) 368.
2. R. Daw and J. Finkelstein, *Nature* **442** (2006) 367.
3. R. Barry and D.J. Ivanov, *J. Nanobiotechnology* **2** (2004) 2.
4. P.S. Dittrich and A. Manz, *Nature Rev. Drug Discovery* **5** (2006) 210.
5. T.M. Squires and S.R. Quake, *Rev. Mod. Physics* **77** (2005) 977.
6. A.D. Stroock, S.K. Dertinger, A. Ajdari, I. Mezic, H.A. Stone, and G.M. Whitesides, *Science* **295** (2002) 647.
7. J.C. McDonald, D.C. Duffy, J.R. Anderson, D.T. Chiu, H. Wu, J.A. Shuller, and G.M. Whitesides, *Electrophoresis* **21** (2000) 27.
8. D.G. Hassell and W.B. Zimmerman, *Chem. Eng. Sci.* **61** (2006) 2977.
9. S.P. Kee and A. Gavriilidis, *Chem. Eng. J.* **142** (2008) 109.
10. C.A. Li and T.N. Chen, *Sens. Actuat. B* **106** (2005) 871.
11. M.S. Williams, K.J. Longmuir, and P. Yager, *Lab on a Chip* **8** (2008) 1121.
12. H. Z. Wang, P. Iovenitti, E. Harvey, and S. Masood, *J. Micromech. Microeng.* **13** (2003) 801.
13. J. Aubin, D.H. Fletcher, and C. Xuereb, *Chem. Eng. Sci.* **60** (2005) 2503.
14. N.S. Lynn and D.S. Dandy, *Lab on a Chip* **7** (2007) 580.
15. J.T. Yang, K.J. Huang, and Y.C. Lin, *Lab on a Chip* **5** (2005) 1140.
16. M. Camesasca, M. Kaufman, and I. Manas-Zloczower, *Macromol. Theory Simul.* **15** (2006) 595.
17. M. Camesasca, M. Kaufman, and I. Manas-Zloczower, *J. Micromech. Microeng.* **16** (2006) 2298.
18. C. Chaktranond, K. Fukagata, and N. Kasagi, *J. Fluid Sci. Technol.* **3** (2008) 1008.
19. M. Camesasca, I. Manas-Zloczower, and M. Kaufman, *J. Micromech. Microeng.* **15** (2005) 2038.
20. M. Itomelenskis, P.S. Fodor, and M. Kaufman, *Eur. Phys. J. Appl. Phys.* **47** (2009) 31301.

21. M. Kaufman and P.S. Fodor, *Physica A* **389** (2010) 2951.
22. M. Kaufman, M. Camesasca, I. Manas-Zloczower, L. A. Dudik, and C. Liu, Applications of Statistical Physics to Mixing in Microchannels: Entropy and Multifractals, in *Proc. of NATO Advanced Study Institute: Functionalized Nanoscale Materials, Devices and Systems for Chem. - Bio. Sensors, Photonics, and Energy Generation and Storage*, Sinaia, Romania, 2007 (Spinger Nato Science for Peace and Security Series Physics and Biophysics, 2007).
23. A. Renyi, *Probability Theory* (Dover Publications, Mineola, NY, 2007).
24. C.E. Shannon, *Bell. Syst. Tech. J.* **27** (1948) 379.
25. W. Wang, I. Manas - Zloczower, and M. Kaufman, *Chem. Eng. Comm.* **192** (2005) 405.
26. T.J. Johnson, D. Ross, and L.E. Locascio, *Anal. Chem.* **74** (2002) 45.
27. A. Wolf, J.B. Swift, H.L. Swinney, and J.A. Vasato, *Physica D* **16** (1985) 285.